Electrochemical ESR and Voltammetric Studies of Lithium Ion Pairing with Electrogenerated 9,10-Anthraquinone Radical Anions Either Free in Acetonitrile Solution or Covalently Bound to Multiwalled Carbon Nanotubes

Andrew J. Wain,[†] Gregory G. Wildgoose,[†] Charles G. R. Heald,[†] Li Jiang,[‡] Timothy G. J. Jones,[‡] and Richard G. Compton*,[†]

Physical and Theoretical Chemistry Laboratory, Oxford University, South Parks Road, Oxford, OX1 3QZ United Kingdom, and Schlumberger Cambridge Research, High Cross, Madingley Road, Cambridge, CB3 0EL United Kingdom

Received: August 13, 2004; In Final Form: October 14, 2004

The influence of lithium ion pairing on the voltammetric reduction of anthraquinone in acetonitrile is reported. On gold electrodes, the single electron reduction generates a radical anion which forms a complex with lithium cations from the electrolyte. In situ ESR studies support this finding, and signal intensity measurements are used to estimate a value for the complexation equilibrium constant. Values calculated were of the of the order of 6000 mol^{-1} dm^3. Potential shift measurements and Digisim modeling are shown to be in support of a complexation mechanism in which a little of the complex precipitates on the electrode surface. The effect of lithium ion pairing is also demonstrated for the case in which 1-anthraquinonyl groups are covalently attached to multiwalled carbon nanotubes abrasively immobilized on a basal plane pyrolytic graphite electrode.

1. Introduction

The importance of electrolyte identity and the influence of ion pairing on the voltammetric reduction of quinones has been the focus of much investigation, particularly in aprotic solvents where the electrochemical reduction takes place in two single electron steps[1−12]

$$Q + e^- \rightleftharpoons Q^{\bullet -} \quad \text{(I)}$$

$$Q^{\bullet -} + e^- \rightleftharpoons Q^{2-} \quad \text{(II)}$$

Cations present in the supporting electrolyte interact with radical anions and dianions formed, the level of their association depending on the identity of both ions and the solvent employed. In the presence of tetraalkylammonium cations in aprotic solvents, for example, it is often assumed that the degree of ion pairing is small enough to be neglected and, hence, their widespread use in electrolyte solutions.[1,2] However, alkali metal cations have a tendency to form complexes with organic anions, which can have a dramatic effect on the observed voltammetry and is manifested in the shifting of voltammetric reduction peaks to less negative potentials as the anions are thermodynamically stabilized by the ion pairing interaction. The extent of this has been found to increase in the order of decreasing cationic radius, suggesting that complex formation is most significant with the Li^+ cation.[1] A large majority of previously documented work concerning ion pairing phenomena in quinone reductions has been carried out in *N*,*N*-dimethylformamide,[1,2,6,8,9,11] possibly to avoid limitations in reagent solubility, and in particular, association constants for the equilibrium between anthraquinone radical anions and lithium cations have been reported.[2,11] However, very few investigations have been undertaken in acetonitrile, and those which have do not report equilibrium constant data.[2,10] The sensitivity of voltammetric redox potentials to differences in the ionic environment means that ion pairing effects are of significant practical interest to the electrochemist, and should therefore be considered when half-wave and peak potentials are reported and mechanisms written.

When paramagnetic anions are generated, electron spin resonance (ESR) provides an elegant method with which to study ion pairing effects in the solution phase, since the observed spectra are often dramatically altered by such ionic associations.[13,14] Metal cations possessing magnetic nuclei often couple with the radical anions such that additional hyperfine splitting arises, and slow cation exchange between equivalent sites on the anion, such as the oxygen atoms in many semiquinones, can result in a line width alternation effect.[13] Ion pairing has been studied using ESR for a number of semiquinones in various solvent systems, in which the radical anions were commonly generated using alkali metal reduction,[15−18] but alternatively by flash photolysis methods.[19]

In this paper, we report the effect of lithium ion pairing on the electrochemical reduction of anthraquinone in acetonitrile. On gold electrodes, the reduction is found to be complicated by the presence of lithium cations in the supporting electrolyte due to the formation of a lithium anthraquinone complex which demonstrates a small degree of insolubility in acetonitrile. Digisim modeling provides further evidence for this mechanism. Simultaneous electrochemical ESR studies using a gold tube flow cell to electrogenerate the radical anions confirm the "titration" of the paramagnetic anthraquinone radical anion with lithium cations, the product of which is ESR invisible. The novel in situ quantification of this "titration" is used to estimate an equilibrium constant for the complexation, which is consistent with that inferred from the Digisim modeling. The electroreduction is also considered for multiwalled carbon nanotubes derivatized with covalently bound 1-anthraquinonyl groups when

* To whom all correspondence should be addressed. E-mail: richard.compton@chemistry.oxford.ac.uk. Tel.: +44 (0) 1865 275 413. Fax: +44 (0) 1865 275 410.
† Oxford University.
‡ Schlumberger Cambridge Research.

10.1021/jp040552u CCC: $30.25
Published on Web 02/15/2005

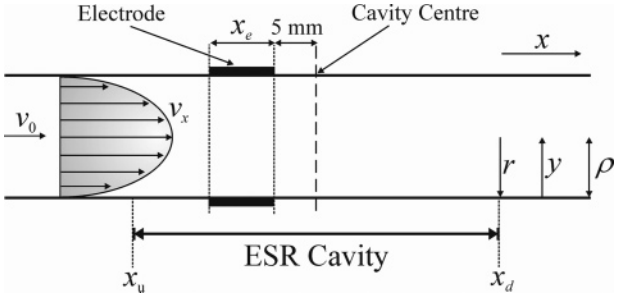

Figure 1. Parabolic flow profile in a tubular flow cell and the relative position of electrode to the ESR cavity (not to scale).

immobilized on a basal plane pyrolytic graphite electrode in which the presence of lithium cations results in the expected reduction potential shift, supporting an ion pairing mechanism.

2. Experimental Section

2.1. Chemical Reagents. All voltammetric experiments were carried out in acetonitrile (Fisions, dried and distilled) with 0.1 M tetrabutylammonium perchlorate (TBAP, Fluka, puriss. electrochemical grade) as supporting electrolyte. In the interests of maintaining a relatively constant ionic strength, in cases where the lithium perchlorate concentration exceeded 10 mM, the concentration of TBAP was adjusted such that the total supporting electrolyte concentration was 0.1 M. 9,10-Anthraquinone and lithium perchlorate (anhydrous) were purchased from Fluka, were of the highest commercially available grade, and were used without further purification.

2.2. Apparatus. Ex situ voltammetry was carried out on a 1 mm diameter gold macrodisk working electrode, with a platinum coil counter electrode (Goodfellow, Cambridge, U.K.). A Ag/$AgNO_3$ reference was constructed from a discarded SCE containing a silver wire (Goodfellow, Cambridge, U.K.) and 10 mM $AgNO_3$ with 0.1 M TBAP in acetonitrile, separated from the bulk solution by a porous frit. Potential control was achieved using a computer controlled PGSTAT30 potentiostat (Autolab, Eco Chemie, Utrecht, The Netherlands). The gold electrode was polished using 1 μm and 0.3 μm alumina (Kemet Ltd., UK). All solutions were degassed with oxygen-free nitrogen (BOC Gases, Guilford, Surrey, U.K.) for at least 15 min prior to experimentation.

In situ electrochemical ESR experiments were carried out using a gold tube flow cell, the construction and characterization of which has been described previously.[20] A platinum gauze counter electrode was positioned downstream of the gold working electrode and a silver wire reference was placed upstream. As a result of the highly resistive nature of the cell design, it was necessary to attach a 0.1 μF capacitor between the reference and counter electrodes in order to maintain potentiostat stability. Fluid motion was maintained using a gravity flow system, employing glass capillaries to achieve slower flow rates. The volume flow rates achieved were in the range 0.1×10^{-3} to 200×10^{-3} cm^3 s^{-1}. The gold electrode surface was cleaned between experiments with 3 micron diamond spray (Kemet International Ltd, U.K.), using a tungsten rod to polish.

ESR spectra were obtained using a JEOL JES−FA100 X-band spectrometer with a cylindrical (TE_{011}) cavity resonator.[14] The cell was positioned in this cavity with the downstream edge of the tube electrode 5 mm from the cavity center, as depicted schematically in Figure 1. Cavity tuning was achieved using the JEOL spectrometer software (A-SYSTEM v.1.100, FA-MANAGER v.1.01), allowing automatic calculation of cavity Q-factor. In all of the experiments, a microwave power of 1 mW was used and in every case a test was run to check that increasing the microwave power increased the ESR signal. Doing so ensured that the system was not power saturated such that the ESR signal intensity gave a direct measure of the number of electrogenerated spins in the cavity.[14] All experiments were conducted at 20 ± 2 °C.

2.3. Derivatization of Multiwalled Carbon Nanotubes (MWCNTs). The covalent derivatization of MWCNTs can be achieved chemically by the reduction of the aryl diazonium salt using hypophosphorous acid as the reducing agent.[21−24] Loss of N_2 from the aryl diazonium salt upon reduction leads to the formation of an aryl radical which is then free to attack the surface of the MWCNT with formation of a covalent bond. The most likely surface sites for attachment of the aryl radicals is at edge-plane or edge-plane-like defect sites on the MWCNT surface.[25,26]

The chemical derivatization of MWCNTs with anthraquinone was achieved using the following protocol: 50 mg of MWCNTs were stirred into 10 cm^3 of a 5 mM solution of Fast Red AL (anthraquinone-1-diazonium chloride), to which 50 cm^3 of hypophosphorous acid (H_3PO_2, 50% w/w in water) was added. Following this, the solution was allowed to stand at 5 °C for 30 min with gentle stirring, after which, the solution was filtered by water suction in order to remove any unreacted species from the MWCNT surface. Further washing with deionized water was carried out to remove any excess acid and finally with acetonitrile to remove any unreacted diazonium salt from the mixture. The derivatized MWCNTs were then air-dried by placing them inside a fume hood for a period of 12 h after which they were stored in an airtight container prior to use.[21−24] The MWCNTs derivatized with anthraquinone were previously characterized as being covalently attached to the surface of the MWCNTs using a voltammetric characterization protocol described in ref 26.

"Bamboo-like" multiwalled carbon nanotubes[27] (purity >95%, diameter 30 ± 15 nm, length 5−20 μm) were purchased from Nano-Lab Inc. (Brighton, MA) and were used without further purification.

Electrochemical measurements were recorded using a μAutolab computer controlled potentiostat (Ecochemie, Utrecht, Netherlands) with a standard three-electrode configuration. All voltammetric experiments were carried out in a glass cell of volume 5 cm^3. A basal plane pyrolitic graphite (bppg, 0.20 cm^2, Le Carbone Ltd, Sussex, U.K.) electrode acted as the working electrode and a platinum coil used as the counter electrode. The cell assembly was completed using a silver wire as a quasi-reference electrode.

3. Theory

3.1. Tubular Electrode. The theory describing simultaneous electrochemical ESR measurements using a tubular flow cell has been reported previously[28] and has been recently developed more fully.[20] The convective diffusion equation for mass transport in a tubular cell is given by[29]

$$\frac{\partial c}{\partial t} = D\left(\frac{\partial^2 c}{\partial x^2} + \frac{\partial^2 c}{\partial r^2} + \frac{1}{r}\frac{\partial c}{\partial r}\right) - v_x\frac{\partial c}{\partial x} \qquad (1)$$

where D is the diffusion coefficient, c is the concentration of the electroactive species, r and x are the radial and axial coordinates, respectively, and v_x is the axial flow velocity. At sufficiently fast flow rates, axial diffusion can be neglected and so the $\partial^2 c/\partial x^2$ term can be removed, and similarly, if we assume

that the diffusion layer of the electrode is thin, it is possible to ignore the radial $1/r$ term. The convection term is considered by introducing a laminar flow profile, shown schematically in Figure 1, which can be simplified under conditions of a thin diffusion layer and reduces eq 1 to[20]

$$\frac{\partial c}{\partial t} = D\frac{\partial^2 c}{\partial y^2} - \frac{2\upsilon_0 y}{\rho}\frac{\partial c}{\partial x} \quad (2)$$

where υ_0 is the axial velocity at the tube center, ρ is the tube radius, and y is the radial coordinate relative to the tube wall. The numerical solution of this simplified mass transport equation yields the Levich equation for the steady-state limiting current (i_{lim}) in the diffusion controlled limit at a tubular electrode[20,30]

$$i_{lim} = 5.24 \times 10^5 n[A]_{bulk} D^{2/3} x_e^{2/3} V_f^{1/3} \quad (3)$$

where n is the number of electrons transferred, $[A]_{bulk}$ is the bulk concentration of electroactive species, D is its diffusion coefficient, x_e is the length of the electrode (3 mm in our case), and V_f is the volume flow rate (given by the integration of the axial flow velocity over the tube radius).

3.2. ESR Signal. ESR signal intensity (S) gives a measure of the total number of spins in the cavity. Thus, by integrating the concentration profile throughout the volume of the cell which is downstream of the electrode (see Figure 1), and by convoluting this with the $\sin^2 x$ sensitivity profile in the ESR cavity,[28] we deduce the following:

$$\text{signal} = S_0 \int_{x_u}^{x_d} \sin^2\left(\frac{x - x_u}{l}\pi\right) \int_0^{\rho} 2\pi r c(r,x)\, dr\, dx \quad (4)$$

where S_0 is the signal measured for one mole of ESR active species at the cavity center, x_u and x_d are the coordinates of the upstream and downstream edge of the cavity, respectively (see Figure 1), l is the length of the cavity, and c is the concentration of the electrogenerated ESR active species.

With a knowledge of the steady-state concentration profile, $c(r,x)$, downstream of the tubular electrode in the ESR cavity, for a given set of experimental conditions, the relative ESR signal intensity S/S_0 can be estimated. Comparison of this with S/S_0 for the case of 100% electrolysis allows a fractional conversion of the starting material to be estimated. This theory is applied in section 4.3 in order to calculate the total concentration of electrogenerated anthraquinone radical anions.

4. Results and Discussion

4.1. Voltammetry on a Gold Macrodisk. The voltammetric reduction of 9,10-anthraquinone (AQ) has been studied extensively on a variety of electrode materials and in a range of solvents.[1,2,5,7,11,31,32] In aprotic solvents, the reduction is known to occur as two reversible single electron steps, generating first the anthraquinone radical anion ($AQ^{\bullet -}$) and second the dianion (AQ^{2-}). Figure 2a depicts the electrochemical reduction of a 2 mM solution of anthraquinone on a 1 mm diameter gold disk electrode in acetonitrile supported with 0.1 M TBAP, at a potential sweep rate of 100 mV s^{-1}, which appears consistent with that described above. The corresponding peak potentials for the first and second reduction steps are -1.26 and -1.80 V vs Ag/Ag^+, respectively, in close agreement with previously reported voltammetry for this solvent and electrode material.[31] Peak currents for both sets of reductive and oxidative waves were found to vary linearly with the square root of the scan rate in the range 50−500 mV s^{-1}, as expected for an electroactive species diffusing in solution.[33]

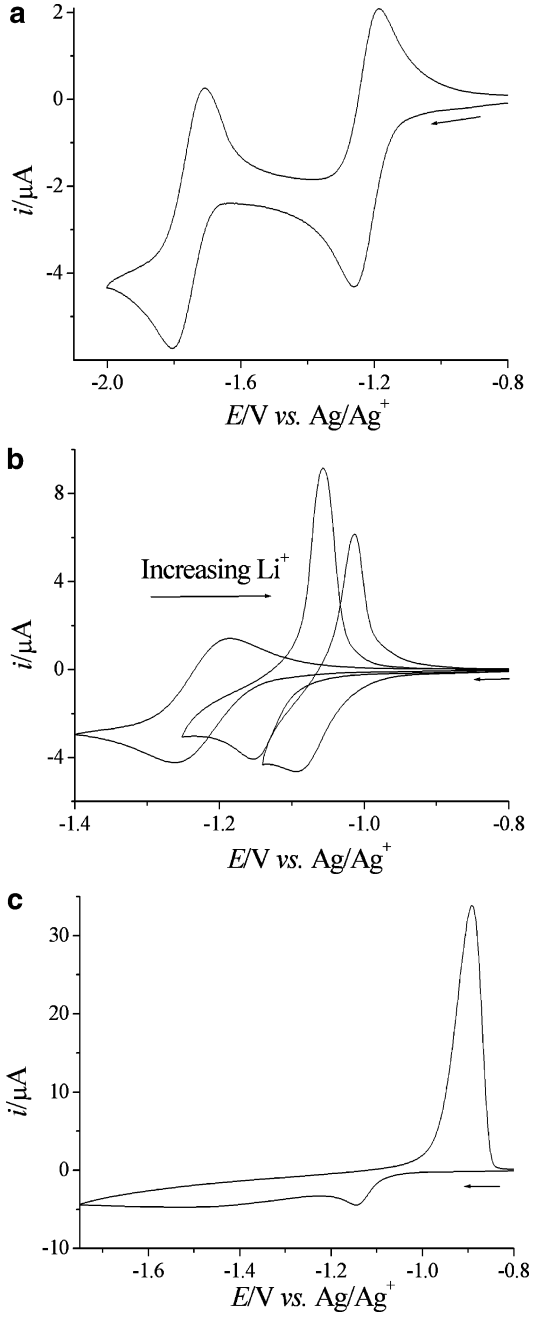

Figure 2. Cyclic voltammograms of 2 mM anthraquinone reduction in acetonitrile supported with 0.1 M TBAP at a scan rate of 100 mV s^{-1}. (a) Two single electron reduction waves in the absence of lithium cations. (b) First reduction waves in the presence of 0 mM $LiClO_4$, 4 mM $LiClO_4$ and 30 mM $LiClO_4$. (c) Both reduction waves in the presence of 5 mM $LiClO_4$.

The addition of lithium cations to the electrolyte has a profound influence on the electrochemical reduction, both in terms of the position of the peak potentials and in the general appearance of the voltammetry. The effect can be seen in Figure 2b, which depicts the $AQ/AQ^{\bullet -}$ redox couple at 100 mV s^{-1}, first in the absence of Li^+ and second in the presence of 4 and 30 mM Li^+, all of which were found to be stable over repetitive cycling. The notable difference is that the reduction and reoxidation peaks are shifted to less negative potentials upon increasing Li^+ concentration, suggesting that the reduction is thermodynamically favored by its presence. Moreover, the shape of the reverse wave is altered significantly by the addition of lithium, becoming much sharper, with an appreciable increase in peak current. The former observation has been well docu-

mented for the electrochemical reduction of a variety of quinones in the presence of alkali metal and alkaline earth metal cations and is attributed to ion pair formation;[1−3,8,10−12] in the presence of just TBAP, there is likely very little association between the electrogenerated anthraquinone radical anion and the tetrabutylammonium cation, whereas strongly coordinating lithium cations demonstrate a high level of ionic association with the electrogenerated radical anion.[1,2] The change in the reverse peak is indicative of the reduced species becoming surface bound, suggesting that some of the ion-paired complex either adsorbs or precipitates onto the gold electrode surface and is "stripped off" during the oxidative scan. The formation of an insoluble lithium salt was reported by Stutts and Eastland for the electrochemical reduction of benzoquinone in acetonitrile[10] so the precipitation of the equivalent anthraquinone salt is plausible under similar conditions. The observed variation in oxidative peak current between the 4 and 30 mM voltammograms can be rationalized by differences in deposition times as a result of the sweep being reversed at different potentials. The process can be described by an EC mechanism, the product of which may precipitate to a limited extent on the electrode

$$AQ_{(MeCN)} + e^- \rightleftharpoons AQ^{\bullet -}_{(MeCN)} \qquad \text{(III)}$$

$$AQ^{\bullet -}_{(MeCN)} + Li^+_{(MeCN)} \rightleftharpoons LiAQ_{(MeCN)} \qquad \text{(IV)}$$

$$LiAQ_{(MeCN)} \rightleftharpoons LiAQ_{(s)} \qquad \text{(V)}$$

Further evidence in support of electrode deposition of the ion-paired complex is apparent when the reductive scan is continued to more negative potentials in order to observe the second electron reduction. This is shown in Figure 2c for the 100 mV s^{-1} reduction of 2 mM anthraquinone, in the presence of 5 mM Li^+. As above, we observe the first single electron reduction at a potential shifted relative to that in the absence of lithium, but the second reduction wave is heavily broadened and the reoxidation occurs as a single wave occurring at a potential significantly less negative than when the scan was reversed before the second reduction. The broadened wave and the large separation between reductive and oxidative peaks suggest that the electron transfer kinetics have become slowed by the presence of lithium, which is consistent with the formation of a partially blocking layer over the gold surface upon the first reduction.[34−36] The fact that the reverse peak still has stripping characteristics suggests that the product of the second reduction is also surface bound. Upon successive cycling, both the reductive and oxidative peaks were found to diminish in magnitude and the peak separation found to increase as the working electrode became progressively more passivated.

It has been established from the above voltammetry that, in the presence of lithium cations, the electrogenerated anthraquinone radical anion becomes ion paired and that some of the complexed radical anions are removed from solution at the electrode surface via precipitation, which suggests that the total number of radical anions that are uncomplexed and essentially "free" in solution is likely to be reduced. Since the radical anion is known to demonstrate a hyperfine ESR spectrum,[16,17,37] it was envisaged that the method of simultaneous electrochemical ESR could be used to provide more information about the ion association equilibrium, and so experiments were carried out using a tubular flow cell for use in generating the radical anions in situ.

4.2. Voltammetry in a Gold Tube Flow Cell. Figure 3a depicts steady-state hydrodynamic voltammograms for the single

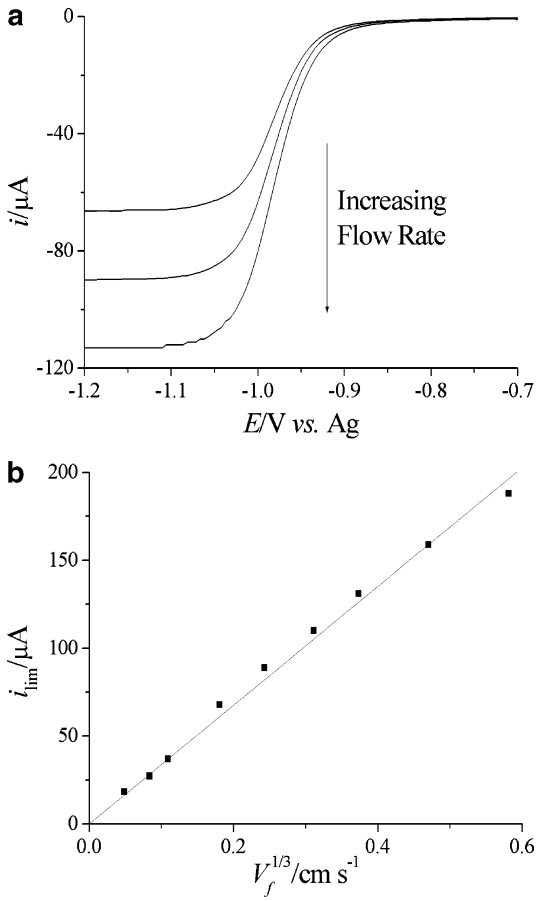

Figure 3. (a) Linear sweep voltammograms depicting the single electron reduction of 2 mM anthraquinone in 0.1 M TBAP supported acetonitrile at a gold tube electrode (scan rate 5 mV s^{-1}). Flow rates shown are 5.9×10^{-3}, 14.4×10^{-3}, and 30.2×10^{-3} cm^3 s^{-1}. (b) Levich plot for the reduction of 2 mM anthraquinone.

electron reduction of 2 mM anthraquinone in acetonitrile supported with 0.1 M TBAP, achieved using a gold tube electrode flow cell which has been described previously.[20] The voltammetry shown corresponds to volume flow rates of 5.9×10^{-3}, 14.4×10^{-3}, and 30.2×10^{-3} cm^3 s^{-1}.

To verify that the flow cell was functioning correctly and that the anthraquinone reduction was behaving according to eq 3, limiting currents were measured at a variety of flow rates in the range 0.1×10^{-3} to 200×10^{-3} cm^3 s^{-1} and were used to construct a Levich plot (Figure 3b). The slope of this plot was used to calculate a diffusion coefficient of 1.94×10^{-5} cm^2 s^{-1}, in good agreement with the literature,[31,32] confirming that the cell was producing a reliable hydrodynamic response.

4.3. ESR Measurement. Figure 4a shows the ESR spectrum obtained when a 0.25 mM solution of anthraquinone (AQ) was electrolyzed in situ at a potential of −1.2 V vs Ag, at a flow rate of $1.3 \times 10^{-4} \pm 0.3 \times 10^{-4}$ cm^3 s^{-1} using the gold tube cell. This low concentration was used in order to minimize line broadening effects due to spin−spin relaxation processes.[14] The spectrum corresponds to that of the anthraquinone radical anion and consists of seventeen lines spread over a field width of 0.6 mT. The measured hyperfine coupling constants of 0.031 and 0.098 mT for the two sets of equivalent protons are in good agreement with the documented values of 0.0303 and 0.0986 mT for anthraquinone radical anions electrogenerated in DMSO at a mercury pool electrode.[37] A simulated spectrum using these hyperfine couplings and a Gaussian line width of 0.015 mT is shown in Figure 4b and displays good qualitative agreement in terms of relative line intensities. It should be noted that hyperfine

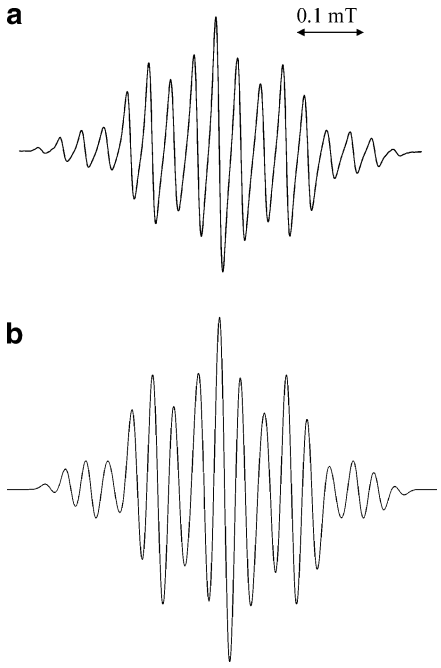

Figure 4. (a) ESR spectrum of anthraquinone radical anion electrogenerated in situ by electrolyzing 0.25 mM anthraquinone in acetonitrile (modulation width 0.005 mT). (b) Simulated spectrum of the anthraquinone radical anion using hyperfine coupling constants from ref 37 and a line width of 0.015 mT.

coupling to two sets of four equivalent protons should result in a total of 25 lines, but since one coupling constant is almost three times the other, a number of lines are unresolved in the spectra shown.

The spectrum obtained upon electrolysis of 0.25 mM anthraquinone at the same flow rate and potential as above, but in the presence of 0.25 mM $LiClO_4$, was found to be qualitatively very similar to that observed in the absence of any Li^+, demonstrating no further hyperfine splitting due to coupling with magnetic ^6Li and ^7Li nuclei, nor any alternating line width effects. The two measured proton hyperfine coupling constants (0.032 and 0.099 mT) were also unchanged within experimental error. However, the signal intensity was found to be considerably diminished by the addition of $LiClO_4$, consistent with the "titration" of Li^+ ions with the electrogenerated anthraquinone radical anions in an EC reaction to produce a complex which could not be detected by ESR. Since the inside of the gold tube electrode is likely shielded from the modulated magnetic field within the ESR cavity, the detection of any paramagnetism arising from the lithium complex precipitated the electrode surface is unlikely. Moreover, the lack of any qualitative change to the spectrum suggests that the solution phase complex is not ESR active. A number of explanations can be offered as to why this may be so. One possibility is the formation of a dimeric complex (such as Li_2AQ_2), which might allow the pairing of the free electrons in the quinone moieties, causing a loss in paramagnetism. This rationale, however, would require a much more complex reaction mechanism which is not supported by the Digisim modeling reported in section 4.4 (vide infra). An alternative possibility is that the ESR signal is broadened by radical anion exchange between free and complexed states. The Gaussian line shapes observed experimentally suggest inhomogeneous signal broadening, possibly reflecting this exchange process. An additional broadening mechanism may also operate as a result of the quadrupolar moments of the ^6Li and ^7Li nuclei.[38] In any case, the ESR signal measures the concentration of "free" or uncomplexed anthraquinone radical anions in solution. With a knowledge of the total radical anion concentration, the variation in signal intensity with Li^+ additions can be used in the estimation of the equilibrium constant, K_{eq}, for the solution complexation reaction.

TABLE 1: Variation of ESR Signal Intensity with Lithium Cation Concentration for the Anthraquinone Radical Anion Electrogenerated in Situ at a Potential of −1.2 V vs Ag and Flow Rate of 1.3×10^{-4} cm^3 s^{-1} [a]

$[Li^+]$/ mM	signal intensity	marker intensity	relative signal	K_{eq}/ mol^{-1}dm^3
0	31 390	440	71	
0.10	23 170	480	48	5500
0.25	14 850	490	30	6000

[a] Signal intensity measurements are reported in arbitrary units.

Table 1 shows signal intensity data measured for the anthraquinone radical anion electrogenerated in situ, in the presence and absence of lithium cations (0.25 mM anthraquinone held at a potential of −1.2 V vs Ag). To maximize signal intensity, the magnetic field was over-modulated to a width of 1 mT. The ESR signal amplitude was measured as the maximum peak-to-peak intensity, in arbitrary units, on the first derivative spectra. To account for changes in cavity Q values between experiments, a manganese (II) marker was used as a standard at the same time anthraquinone measurements were being made. The ratio of signal to marker intensity was then used in the calculation outlined below.

The equilibrium constant, K_{eq}, for the solution phase ion association step, IV, is defined by

$$K_{eq} = \frac{[LiAQ]_{MeCN}}{[Li^+]_{Free}[AQ^{\bullet -}]_{Free}} \quad (5)$$

where $[Li^+]_{Free}$ and $[AQ^{\bullet -}]_{Free}$ are the concentrations of the free ions in solution. The total concentration of the lithium cation and the anthraquinone radical anion are given by

$$[Li^+]_{Tot} = [LiAQ]_{MeCN} + [Li^+]_{Free} \quad (6)$$

and

$$[AQ^{\bullet -}]_{Tot} = [LiAQ]_{MeCN} + [AQ^{\bullet -}]_{Free} \quad (7)$$

We know the value of $[Li^+]_{Tot}$ for the experiments conducted, and the ESR signal intensity gives a measure of $[AQ^{\bullet -}]_{Free}$, but a knowledge of $[AQ^{\bullet -}]_{Tot}$ is also required in order to estimate K_{eq}. So it is necessary to determine the fractional conversion of the starting anthraquinone at the electrode. In our previous work where the tubular cell was characterized,[20] a computer program was written to simulate the ESR signal intensity under a specific set of conditions based on the theory outlined in section 3. Comparing the simulated signal intensity at this flow rate to that calculated for 100% anthraquinone reduction allowed a conversion of 12% to be estimated, corresponding to $[AQ^{\bullet -}]_{Tot} = 0.031$ mM. Using this, and the tabulated signal intensities with their corresponding lithium concentrations, a simultaneous solution of eqs 5−7 allowed two values for K_{eq} to be calculated, as shown in Table 1. It is important to note that, although some small precipitation effects are observable in the macrodisk voltammetry, we assume such effects are negligible in the evaluation of K_{eq}, since the ESR signal is stable with time.

Pletcher and Thompson reported an association constant of 560 mol^{-1} dm^3 between lithium cations and anthraquinone radical anions in DMF,[11] approximately an order of magnitude less than calculated above. This is not unexpected, since DMF

likely to be significantly better at solvating the ions than acetonitrile; the mole fraction solubility of lithium perchlorate, for example, has been reported as 0.059 in acetonitrile, but 0.340 in DMF.[39] It is also important to note that the above authors did not report any observations suggesting the precipitation of the lithium anthraquinone complex.[11] Based on this, and the results outlined above, we can postulate that the lithium salt of the anthraquinone radical anion has a relatively low solubility in acetonitrile (cf. DMF) and precipitates onto the electrode surface during the electroreduction on the cyclic voltammetric time scale, but deposition is not a continuous process and is therefore not significant once steady-state concentrations are achieved.

Next, we discuss more fully the quantitative effect that lithium cations were found to have on the voltammetric reduction and describe the use of Digisim modeling to provide further evidence for the mechanism suggested above.

4.4. Lithium Concentration Dependence and Digisim Modeling. Consider the electroreduction of anthraquinone in the presence of lithium cations

$$AQ + Li^+ + e^- \rightleftharpoons LiAQ \qquad (VI)$$

Under equilibrium conditions, the reduction potential for this redox reaction is given by the Nernst equation

$$E = E_0 - \frac{RT}{F} \ln \frac{[LiAQ]}{[Li^+][AQ]}$$

where E_0 is the standard anthraquinone reduction potential. From this, we expect the reduction to shift to more positive potentials by 58 mV per decadic increase in lithium cation concentration at 20 °C,[33,40] and so experiments were carried out with lithium perchlorate concentrations in the range 2−0.1 M, with an anthraquinone concentration of 2 mM. The variation of the $AQ/AQ^{\bullet -}$ reduction peak potential with lithium concentration can be seen in Figure 5a. Potentials have been plotted as a shift, ΔE, relative to the anthraquinone reduction peak potential in the absence of any lithium. This was necessary since over long periods of time the reduction potentials were found to drift by as much as 10 mV, possibly due to instability with the reference electrode, so occasionally, a voltammogram was recorded with anthraquinone in the absence of lithium cations, to reduce the effects of this. The slope of the plot in Figure 5a is found to approach 58 mV per decade at high lithium concentrations, suggesting Nernstian behavior. The deviation from the expected slope at low lithium concentrations can be rationalized in terms of depletion effects: On the right-hand side of the plot, the lithium ions are in a large excess of the anthraquinone molecules, and so there is a large reservoir for the radical anions to react with; however, toward the left, the two species are approaching a similar concentration, and there are not enough cations to ion pair with the anthraquinone radical anions, causing a deviation from equilibrium behavior. Further depletion effects are seen at an even lower concentration and will be described later.

As an aside, it was of interest to look at how the second reduction peak potential varied with lithium concentration, which can be seen in Figure 5b. The large degree of scatter in the plot is due to uncertainty in the peak potential as a result of the second reduction wave being so broad and the fact that this reduction is likely to be highly dependent upon the extent of electrode fouling as a result of the first reduction. The points to note are that the slope of this plot is close to 200 mV per Li^+ decade, suggesting that a much more complex mechanism takes place during this second electron reduction, and as a result,

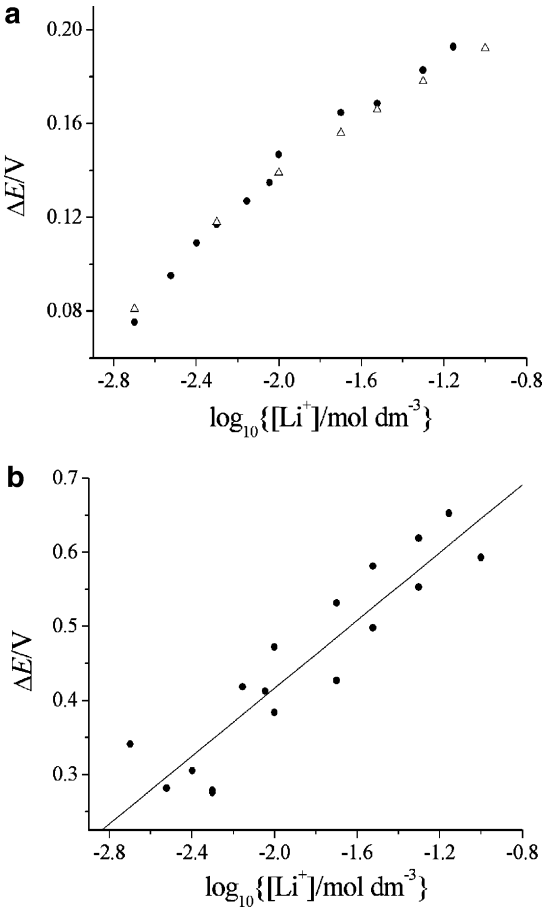

Figure 5. Plots showing the variation of reduction peak potential shift, ΔE (see text) with lithium cation concentration. (a) First reduction peak (●, experimental data; Δ, simulated data − see text). (b) Second reduction peak.

the separation between the first and second reduction peaks decreases upon lithium addition. In fact, in 0.1 M $LiClO_4$, the two waves were found to coalesce into a single two electron reduction. It is interesting to draw the analogy to the reduction of quinones in aqueous media, where a single two electron wave is observed due to protonation steps.[1,5] In this case, Li^+ is acting as a Lewis acid and effectively mimics the behavior of protons in aqueous solution.[3] The larger shift in the second reduction potential with lithium concentration has been observed for anthraquinone in DMF and was attributed to the strong ionic interaction rendering the process irreversible.[1]

Next, we modeled the observed behavior using Digisim.[41] Figure 6 depicts the experimental single electron reduction of 2 mM anthraquinone, with simulated data overlayed. Parameters used for the fit were $E_{1/2} = -1.22$ V, $\alpha = 0.5$, $k_0 = 0.8$ cm s^{-1} (taken from ref 32), scan rate = 100 mV s^{-1} and $D = 1.9 \times 10^{-5}$ cm^2 s^{-1} for both the parent and the reduced species, as calculated in section 4.2. The effect on the reduction potential of adding a homogeneous reaction step, corresponding to the complexation equilibrium, was investigated using 5700 mol^{-1} dm^3 as the equilibrium constant. Difficulty arose, with respect to treatment of the model using Digisim, in trying to account for the fact that the product of the chemical step is partially insoluble in our proposed mechanism and was therefore quickly being removed from the chemical equilibrium. A solution to this problem was found by first maximizing the rate of the forward homogeneous reaction, using a diffusion controlled rate constant ($k_f = 10^{11}$ mol^{-1} dm^3 s^{-1}) and then mimicking the precipitation by assigning a very high, fictitious diffusion

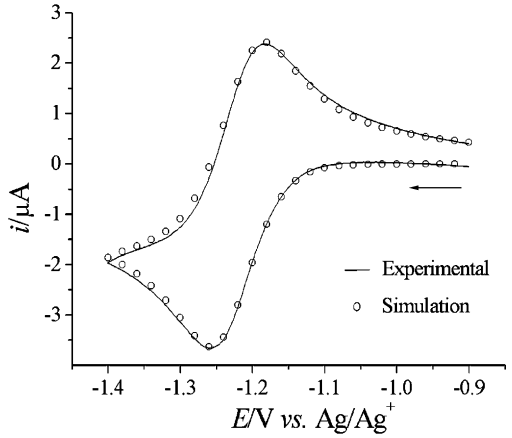

Figure 6. Digisim fit of the single electron reduction of 2 mM anthraquinone using the following parameters: $E_{1/2} = -1.22$ V, $\alpha = 0.5$, $k_0 = 0.8$ cm s^{-1}, scan rate = 100 mV s^{-1}, $D = 1.9 \times 10^{-5}$ cm^2 s^{-1} for both anthraquinone and its radical anion, 2 kΩ uncompensated resistance.

coefficient to the lithium anthraquinone complex ($D = 5 \times 10^{-4}$ cm^2 s^{-1}). Although this may seem counterintuitive, since precipitation of the complex involves immobilization on the electrode surface, using this high value forces the product of the chemical step to be removed very quickly from the reaction layer, as if it were chemically unreactive. The results of the simulation using the parameters given above, and a Li^+ diffusion coefficient of 2.5×10^{-5} cm^2 s^{-1}, are plotted in Figure 5a and are found to be in good agreement with the experimental data, including the depletion effects at low Li^+ concentration. Due to the likely complexity of the precipitation, no attempt was made to model the second reduction step, nor the reverse peaks.

Further investigations into the depletion effects at low Li^+ concentrations were carried out using Digisim for lithium concentrations in the range 0−2 mM ([AQ] = 2 mM), and the modeled voltammograms are depicted in Figure 7a. At very low Li^+ concentrations, the voltammetric response appears to occur as a split wave, the first peak of the wave increasing in magnitude with increasing [Li^+] and the second peak decreasing, until we reach 2 mM Li^+, where the second wave is completely lost. The effect is also observed experimentally as can be seen in Figure 7b, which further supports the proposed mechanism. This phenomenon can be explained by the titration of the lithium cations with electrogenerated anthraquinone radical anions during the first shoulder of the wave, up to the point at which no Li^+ remains in solution to react and so we then see the wave expected in the absence of Li^+, which is diminished in magnitude. It is only when the Li^+ concentration is as high as that of the anthraquinone (2 mM), so that we no longer see any contribution from the reduction of the "free" anthraquinone, without the effects of any ion pairing.

4.5. Anthraquinone Derivatized Multiwalled Carbon Nanotubes (MWCNTs). In the final part of this investigation, we describe the effect of lithium cations on the electrochemical behavior of multiwalled carbon nanotubes (MWCNTs) chemically modified with anthraquinone. These MWCNTs are described as "bamboo-like" in which the axis of the graphite planes is at an angle to the axis of the carbon nanotube, analogous to "paper cups stacked one inside the other".[27] As such, the number of edge-plane like defects on the surface is high, leading to a high surface activity and numerous sights for the anthraquinonyl radical to bind to the MWCNT during the homogeneous derivatization procedure.

The voltammetric reduction of anthraquinone derivatized nanotubes abrasively immobilized on a basal plane pyrolytic

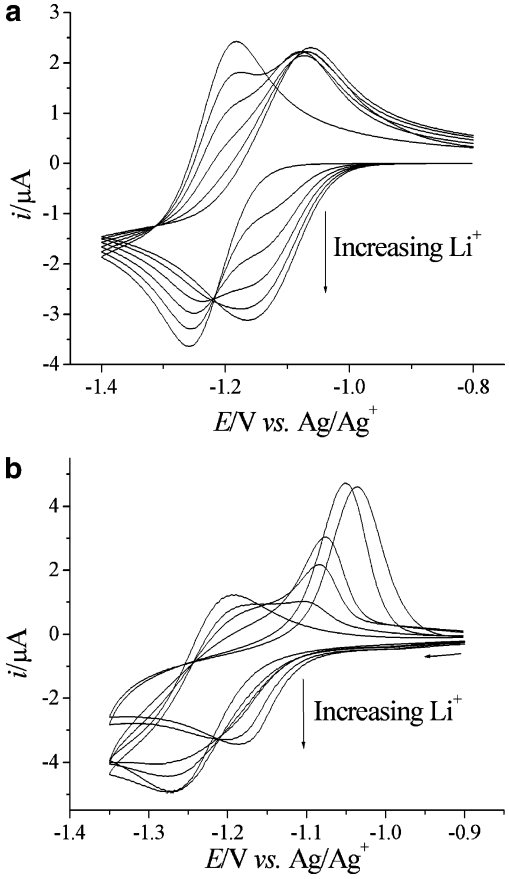

Figure 7. (a) Simulated voltammograms depicting the splitting of reduction waves at low concentrations of lithium cations. [Li^+] = 0.0, 0.4, 0.8, 1.2, 1.6, and 2.0 mM. (b) Experimental cyclic voltammograms demonstrating the low concentration split wave phenomenon. [Li^+] = 0.0, 0.6, 0.8, 1.0, 1.4, and 1.8 mM.

graphite electrode immersed in acetonitrile containing 0.1 M TBAP is depicted in Figure 8a, for a scan rate of 100 mV s^{-1}. A single electron quasireversible wave is observed which remains relatively stable upon successive cycling. For an electroactive species immobilized on an electrode surface, the peak current is expected to be proportional to the potential sweep rate employed.[33] However, variable scan rate experiments revealed a deviation from this predicted trend, and both oxidative and reductive peak currents were found to be proportional to the square root of the scan rate. This does not necessarily imply that the anthraquinone molecules have become detached from the nanotubes on the electrode surface but could also be rationalized by the motion of charge across the surface of the solid carbon nanotubes via an electron hopping mechanism from one immobilized anthraquinone group to another, giving rise to diffusive characteristics in the voltammetry. This phenomenon has been observed in previous work[25,26] in which the possibility of electroactive material becoming detached from the electrode was ruled out; voltammetric signals were stable over repetitive scanning and remained so when the electrode surface was gently rinsed and re-immersed into fresh electrolyte solution, suggesting that the electroactive material was not in the solution phase.

The addition of lithium to the electrolyte was found to affect the electrochemical reduction of the anthraquinonyl derivatized nanotubes in a similar way to the solution phase behavior, with the reduction wave shifting to less negative potentials with increasing Li^+ concentration. As shown in Figure 8b, the peak potential was found to vary linearly with the log of Li^+ concentration, with a slope of 61 mV per Li^+ decade, which is

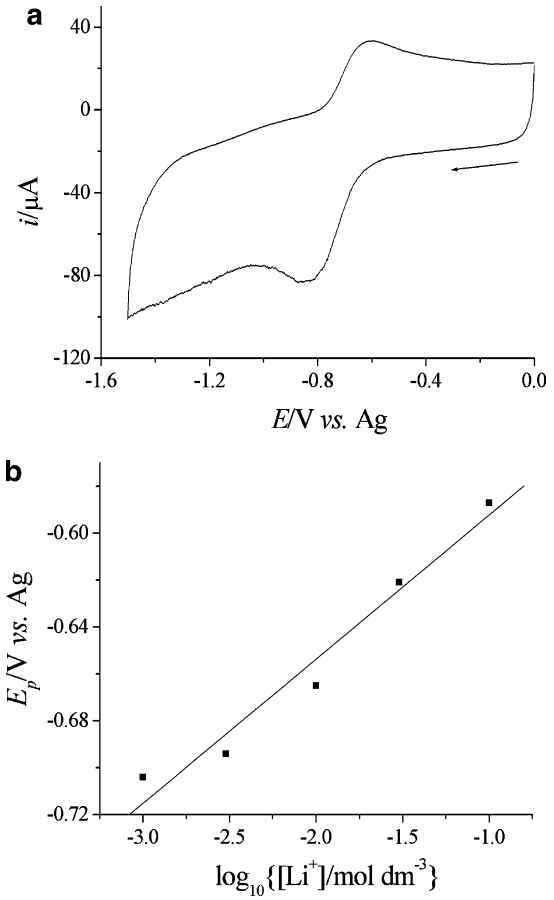

Figure 8. (a) Cyclic voltammogram depicting the reduction of anthraquinone derivatized on MWCNTs on a bppg electrode in acetonitrile supported with 0.1 M TBAP at a scan rate of 100 mV s^{-1}. (b) Variation of the first reduction peak potential with lithium cation concentration.

again consistent with the EC mechanism in which the electrogenerated anthraquinone radical anions become ion paired with lithium cations. However, no electrode passivation effects were observed, suggesting that in contrast to the solution phase electrochemistry on gold electrodes, the electrogenerated anthraquinone radical anions interact with Li^+ cations, but the $Li^+AQ^{\bullet-}$ ion pairs remain chemically attached to the carbon surface as individual moieties, rather than as a solid precipitate.

5. Conclusions

We have reported how lithium ion pairing influences the voltammetric reduction of anthraquinone in acetonitrile initially on gold electrodes and then in the form of multiwalled carbon nanotubes chemically modified with anthraquinone. On gold, the single electron reduction generates the anthraquinone radical anion which, in the presence of lithium cations, forms a complex of limited solubility in acetonitrile. This is in contrast to previous work in DMF in which no effects due to low solubility were reported.[2,11] ESR studies confirmed the removal of ESR active species from the solution phase via complexation, and signal intensity data allowed the estimation of an equilibrium constant for the complexation. Digisim modeling provided further evidence for the proposed mechanism. Finally, lithium ion-pairing was found to shift the reduction potential for anthraquinone when chemically bound to multiwalled carbon nanotubes, suggesting that ionic association phenomena are not confined to solution phase materials.

Acknowledgment. A.J.W. thanks the EPSRC and JEOL, and G.G.W. thanks the BBSRC and Schlumberger Cambridge Research for financial support.

References and Notes

(1) Peover, M. E. *Electroanalytical Chemistry*; Marcel Dekker: New York, 1962; Vol. 2.

(2) Peover, M. E.; Davies, J. D. *J. Electroanal. Chem.* **1963**, *6*, 46.

(3) Eggins, B. R. *Chem. Commun.* **1969**, 1267.

(4) Parker, V. D. *Chem. Commun.* **1969**, 716.

(5) Mann, C. K.; Barnes, K. K. *Electrochemical Reactions in Non-Aqueous Systems*; Marcel Dekker: New York, 1970.

(6) Tkalcec, M.; Filpovic, I.; Piljac, I. *Anal. Chem.* **1975**, *47*, 1773.

(7) Rosanske, T. W.; Evans, D. H. *J. Electroanal. Chem* **1976**, *72*, 277.

(8) Nagaoka, T.; Okazaki, S.; Fujinaga, T. *J. Electroanal. Chem* **1982**, *133*, 89.

(9) Russel, C.; Jaenicke, W. *J. Electroanal. Chem* **1986**, *199*, 139.

(10) Stutts, K. J.; Eastland, G. W. *J. Electroanal. Chem* **1987**, *235*, 357.

(11) Pletcher, D.; Thompson, H. *J. Chem. Soc., Faraday Trans.* **1998**, *94*, 3445.

(12) Oyama, M.; Marken, F.; Webster, R. D.; Cooper, J. A.; Compton, R. G.; Okazaki, S. *J. Electroanal. Chem* **1998**, *451*, 193.

(13) Symons, M. C. R. *J. Phys. Chem.* **1967**, *71*, 172.

(14) Weil, J. A.; Bolton, J. R.; Wertz, J. E. *Electron Paramagnetic Resonance, Elementary Theory and Practical Applications*; John Wiley and Sons: New York, 1994.

(15) Lucken, E. A. C. *J. Chem. Soc.* **1964**, 4234.

(16) Rutter, A. W.; Warhurst, E. *Trans. Faraday Soc.* **1968**, *64*, 2338.

(17) Gough, T. E.; Hindle, P. R. *Trans. Faraday Soc.* **1970**, *66*, 2420.

(18) Allendoerfer, R. D.; Papez, R. J. *J. Phys. Chem.* **1972**, *76*, 1012.

(19) Gough, T. E.; Symons, M. C. R. *Trans. Faraday Soc.* **1966**, *62*, 269.

(20) Wain, A. J.; Thompson, M.; Klymenko, O. V.; Compton, R. G. *Phys. Chem. Chem. Phys.* **2004**, *6*, 4018.

(21) Pandurangappa, M.; Lawrence, N. S.; Compton, R. G. *Analyst* **2002**, *127*, 1568.

(22) Pandurangappa, M.; Lawrence, N. S.; Jiang, L.; Jones, T. G. J.; Compton, R. G. *Analyst* **2003**, *128*, 473.

(23) Wildgoose, G. G.; Pandurangappa, M.; Lawrence, N. S.; Jiang, L.; Jones, T. G. J. *Talanta* **2003**, *60*, 887.

(24) Leventis, H. C.; Streeter, I.; Wildgoose, G. G.; Lawrence, N. S.; Jiang, L.; Jones, T. G. J.; Compton, R. G. *Talanta* **2004**, *63*, 1039.

(25) Wildgoose, G. G.; Wilkins, S. J.; Williams, G. R.; France, R. R.; Carnahan, D. L.; Jiang, L.; Jones, T. G. J.; Compton, R. G. *ChemPhysChem* **2005**, *6*, 352.

(26) Heald, C. G. R.; Wildgoose, G. G.; Jiang, L.; Jones, T. G. J.; Compton, R. G. *ChemPhysChem* **2004**, *5*, 1794.

(27) Wang, Y. T.; Tang, G. Y.; Koeck, F. A. M.; Brown, B.; Garguilo, J. M.; Nemanich, R. J. *Diamond Relat. Mater.* **2004**, *13*, 1287.

(28) Albery, J. W.; Chadwick, A. T.; Coles, B. A.; Hampson, N. A. *J. Electroanal. Chem* **1977**, *75*, 229.

(29) Levich, V. G. *Physicochemical Hydrodynamics*; Prentice-Hall: New York, 1962.

(30) Blaedel, W. J.; Olson, C. L.; Sharma, L. R. *Anal. Chem.* **1963**, *35*, 2100.

(31) Howell, J. O.; Wightman, R. M. *Anal. Chem.* **1984**, *56*, 524.

(32) Samuelsson, R.; Sharp, M. *Electrochim. Acta* **1978**, *23*, 315.

(33) Bard, A. J.; Faulkner, L. R. *Electrochemical Methods, Fundamentals and Applications*, 2nd ed.; John Wiley and Sons: New York, 2001.

(34) Amatore, C.; Saveant, J.-M.; Tessier, D. *J. Electroanal. Chem.* **1983**, *147*, 39.

(35) Brookes, B. A.; Davies, T. J.; Fisher, A. C.; Evans, R. G.; Wilkins, S. J.; Yunus, K.; Wadhawan, J. D.; Compton, R. G. *J. Phys. Chem. B* **2003**, *107*, 1616.

(36) Davies, T. J.; Moore, R. R.; Banks, C. E.; Compton, R. G. *J. Electroanal. Chem.* **2004**, *574*, 123.

(37) Stone, E. W.; Maki, A. H. *J. Chem. Phys.* **1962**, *36*, 1944.

(38) Cederberg, J.; Olson, D.; Larson, J.; Rakness, G.; Jarausch, K.; Schmidt, J.; Borovsky, B.; Larson, P.; Nelson, B. *Phys. Rev. A* **1998**, *57*, 2539.

(39) Markowitz, M. M.; Hawley, W. N.; Boryta, D. A.; Harris, R. F. *J. Chem. Eng. Data* **1961**, *6*, 325.

(40) Saveant, J.-M. *J. Phys. Chem. B* **2001**, *105*, 8995.

(41) Rudolph, M.; Reddy, D. P.; Feldberg, S. W. *Anal. Chem.* **1994**, *66*, 589A.